How to cite: *Angew. Chem. Int. Ed.* **2025**, *64*, e202419195
doi.org/10.1002/anie.202419195

Gas Sensors

Energy-Level Alignment at TiO_2@NH_2-MIL-125 Interface for High-Performance Gas Sensing

Wei-Hua Deng, Min-Yi Zhang, Chun-Sen Li, Ming-Shui Yao,* and Gang Xu**

Abstract: Metal oxide (MO)-based chemiresistive sensors have great potential in environmental monitoring, security protection, and disease diagnosis. However, the thermally activated sensing mechanism in pristine MOs leads to high working temperature and poor selectivity, which are the main challenges impeding practical applications. Precise modulation of the band structure at the heterojunction interfaces of MOs offers the opportunity to unlock unique electrical and optical properties, enabling us to overcome these challenges. Metal–organic frameworks (MOFs) with tunable structures are promising materials for aligning the energy levels at the heterojunctions of MOs. Herein, we report the energy-level structural engineering of MO@MOF heterojunctions to optimize chemiresistive sensing performance. The interface was flexibly modulated from a straddling gap to a staggered gap by -NH_2 functionalization of TiO_2@$(NH_2)_x$-MIL-125, varying x from 0 to 1 and 2, respectively. TiO_2@$(NH_2)_x$-MIL-125 combines the advantages of MOs and MOFs to synergistically improve gas-sensing properties. As a result, TiO_2@NH_2-MIL-125 is the first light-activated material to detect NO_2 at 1 ppb with a response time of < 0.3 min at room temperature. It also exhibited excellent selectivity and long-term stability. Our study underscores the potential of energy band engineering in creating high-performance sensors, offering a strategy to overcome current material limits.

Introduction

Chemiresistive gas sensors have sparked considerable interest in healthcare, industrial safety, air quality monitoring, wearable devices, and other fields.[1] Metal oxides (MOs) are crucial sensing materials in chemiresistive sensors owing to their rapid response, robustness, and low cost.[2] However, the poor selectivity and high operating temperature (> 200 °C) hinder their applications.[3] Heterojunctions represent a crucial domain in materials science.[4] The heterojunction strategy can regulate the energy band structure of materials, thereby inducing unique electrical and optical properties, such as tunneling and quantum confinement effects.[5] It enables the development of more efficient and sensitive electronic and optoelectronic devices.[6] Forming heterojunctions between MOs and other materials has the potential to facilitate the transport of photons and electrons, thereby addressing the challenges currently facing chemiresistive sensors.

Metal–organic frameworks (MOFs) are a class of crystalline porous materials assembled through the coordination of metal (clusters) and organic ligands.[7] Their high porosity, designable structures, and ease of functionalization have garnered widespread attention over the past decade.[8] Recent studies have demonstrated that the integration of MOFs with other materials to create heterostructures can enhance their performance across various applications, including drug delivery, photocatalysis, and chemical sensing.[9] For instance, we fabricated a ZnO@ZIF-CoZn core-sheath nanowire array heterojunction that combines the hydrophobic properties of MOFs with the gas-sensing performance of ZnO for use in acetone sensors with exceptional water resistance.[10] Subsequently, we designed and prepared a TiO_2@NH_2-MIL-125 (MIL: material from Institute Lavoisier) core-sheath nanowire arrays, which not only generated photoexcited charge carriers under visible light but also shortened the diffusion path of charge carriers and enriched target molecules at the heterostructure interface.[11] This heterojunction shows unparalleled capabilities in the detection of the explosive RDX, surpassing

[*] Dr. W.-H. Deng
Fujian Provincial Key Laboratory of Polymer Materials, College of Chemistry and Materials Science, Fujian Normal University, Fuzhou 350007 (China)
Dr. W.-H. Deng, Dr. M.-Y. Zhang, Prof. C.-S. Li, Prof. M.-S. Yao, Prof. G. Xu
State Key Laboratory of Structural Chemistry, Fujian Institute of Research on the Structure of Matter, Chinese Academy of Sciences, Fuzhou, Fujian 350002 (China)
E-mail: gxu@fjirsm.ac.cn
chunsen.li@fjirsm.ac.cn
msyao@ipe.ac.cn
Prof. M.-S. Yao
State Key Laboratory of Mesoscience and Engineering, Institute of Process Engineering, Chinese Academy of Sciences, Beijing 100190 (China)
Prof. G. Xu
Fujian Science & Technology Innovation Laboratory for Optoelectronic Information of China, Fuzhou, Fujian 350108 (China)
Prof. M.-S. Yao, Prof. G. Xu
University of Chinese Academy of Sciences, Beijing 100049 (China)
Prof. C.-S. Li
Fujian Provincial Key Laboratory of Theoretical and Computational Chemistry, Xiamen, Fujian 361005, China

traditional sniffer dogs. Despite the immense potential of core-sheath nanowire array heterojunctions in enhancing gas-sensing performance, systematic research on interfacial band alignment is currently lacking. This gap severely restricts performance improvement and application expansion of such heterostructure materials.

NO_2 is not only a crucial gas in the rocket-launching process but also an air pollutant that poses a threat to the environment and human health.[12] The ability to detect NO_2 with high selectivity at room temperature (RT), without the need for a heating element, has significant implications for both safety and energy conservation. Therefore, NO_2 was selected as the target analytical gas to demonstrate the feasibility of the material design strategy. In this work, we report the first-ever energy-level structural engineering of MO@MOF core-sheath nanowire array heterojunctions, aimed at optimizing chemiresistive gas-sensing performance. Hendon et al. reported that the band gap of MIL-125 could be tuned from 3.6 to 1.3 eV by functionalizing the 1,4-benzenedicarboxylate (bdc) linker with $-NH_2$ groups.[13] Inspired by these studies, we selected MIL-125 for the growth on a TiO_2 nanowire array to form a well-defined TiO_2@MIL-125 sensing interface. The energy-level structure of this sensing interface was flexibly modulated from a straddling gap to a staggered gap by varying the number of $-NH_2$ groups within the MIL-125 framework. This fine tuning improved the efficiency of photoelectron conversion at the MO@MOF interface, enhancing the light-activated sensing performance of TiO_2@MIL-125 in terms of both sensitivity and selectivity. Consequently, the light-activated sensing material simultaneously possesses a limit of detection (LOD) of 1 ppb and a NO_2 response time of < 0.3 min at RT. Moreover, this material shows excellent NO_2 selectivity and long-term stability for over a year.

Results and Discussion

Bandgap engineering and the incorporation of functional groups endow MO@MOF heterojunction materials with adjustable electron-transport properties, facilitating the creation of optimal gas-sensing materials tailored for target gas molecules. Scheme 1 shows the solvothermal growth of MOF thin films, $(NH_2)_x$-MIL-125 (x = 0, 1, or 2), on TiO_2 nanowire arrays (NWAs); this structure is denoted TiO_2@-$(NH_2)_x$-MIL-125 (x = 0, 1, or 2). TiO_2@$(NH_2)_x$-MIL-125 core-sheath NWAs were precisely fabricated by the in situ growth of a layer of $(NH_2)_x$-MIL-125 thin films on the TiO_2 NWA substrate via a two-step seed-assisted solvothermal process (for details, see Experimental Section). The scanning electron microscopy (SEM) and transmission electron microscopy (TEM) images of the TiO_2 NWAs and TiO_2@-$(NH_2)_x$-MIL-125 core-sheath NWAs on Al_2O_3 substrates are shown in Figures 1 and S1–5. As can be seen, the TiO_2 NWAs were obtained via the solvothermal method (Figures S1, 2),[14] then they were sequentially immersed into a solution of bdc-$(NH_2)_x$ ligand (bdc = 1,4-benzene dicarboxylates; bdc-NH_2 = 2-aminobenzene dicarboxylate; bdc-$(NH_2)_2$ = bdc-NH_2 and 2,5-diaminobenzene dicarboxylate in the ratio of 9:1) for 12 h and then into titanium n-butoxide solution for a further 4 h at 150 °C. A rinse process with MeOH, DMF and then MeOH again was performed to remove unreacted reagents from these two immersion steps. These modification steps can provide the crystalline nuclei of MOF, playing a critical role in ensuring homogeneous

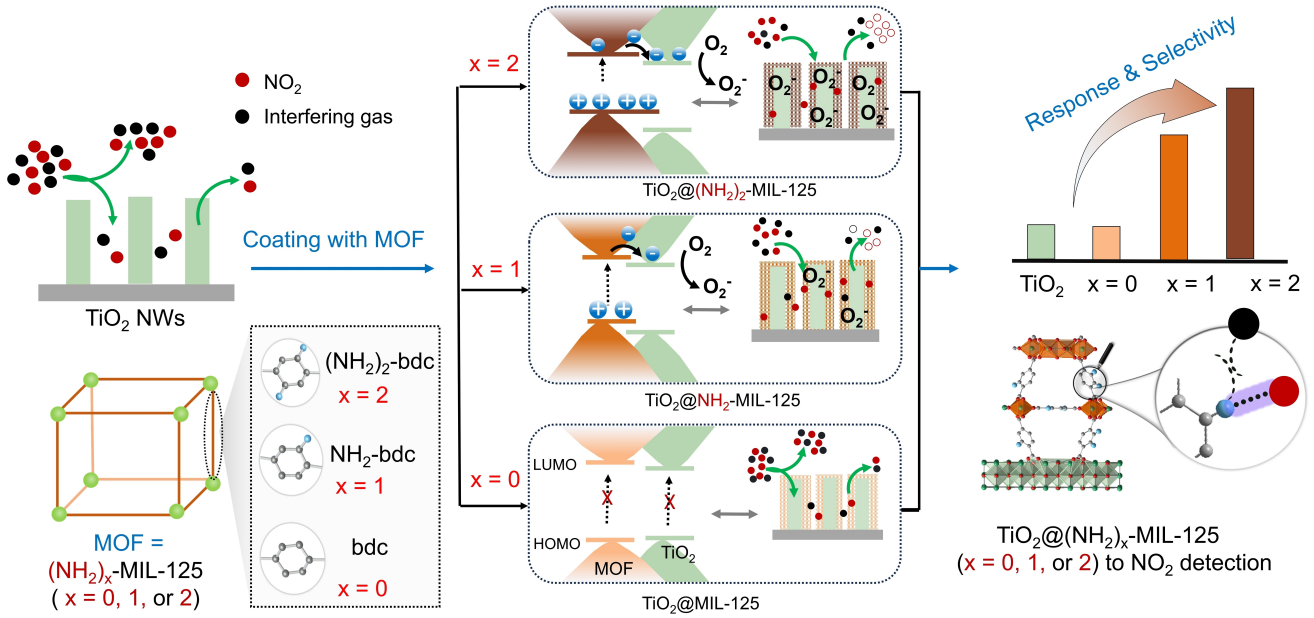

Scheme 1. Schematic procedure for the design of the TiO_2@$(NH_2)_x$-MIL-125 (x = 0, 1, or 2) gas sensing materials through band gap-match modification, inset: schematic energy band diagram depicts the separation processes of photoexcited charge carriers taking place within the MO@MOF interface.

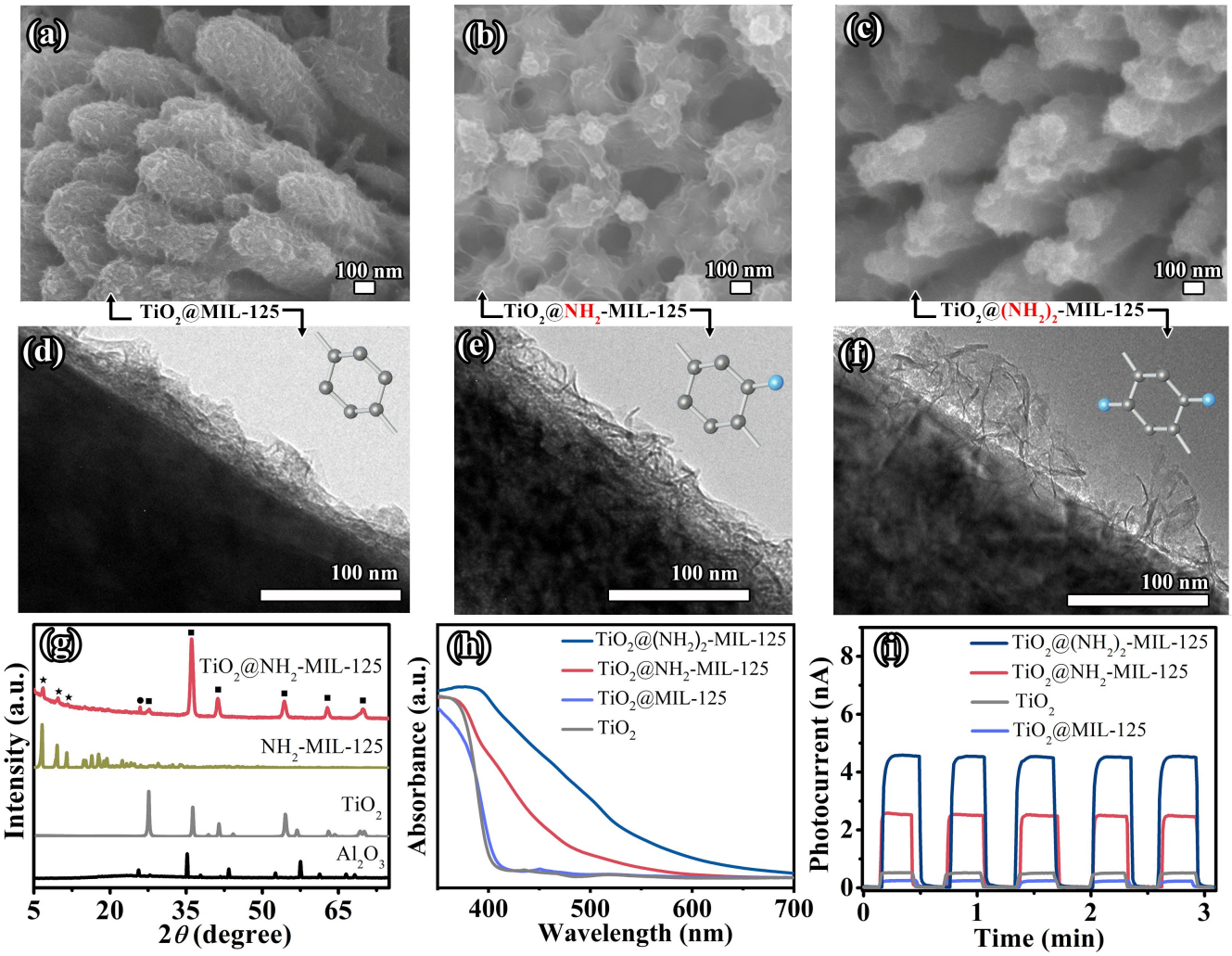

Figure 1. SEM and TEM images of (a and d) TiO_2@MIL-125, (b and e) TiO_2@NH_2-MIL-125, and (c and f) TiO_2@$(NH_2)_2$-MIL-125. (g) PXRD patterns of Al_2O_3 substrate, TiO_2, NH_2-MIL-125 and TiO_2@NH_2-MIL-125 on Al_2O_3 substrate (star: NH_2-MIL-125; circle: Al_2O_3 substrate; square: TiO_2); (h) UV/Vis spectra of TiO_2 and TiO_2@$(NH_2)_x$-MIL-125 on Al_2O_3 substrate; (i) Transient photocurrent response of TiO_2 and TiO_2@$(NH_2)_x$-MIL-125 under visible light..

and continuous growth of the MOF thin film during the subsequent processes. In the absence of these steps, NH_2-MIL-125 particles mainly form in the solution, resulting in phase segregation of TiO_2 nanowires and MOF sheets (Figure S3).

The nuclei-modified TiO_2 NWAs were then immersed in a solution containing bdc-$(NH_2)_x$ and titanium n-butoxide, within a Teflon-lined autoclave and maintained at 150 °C for 72 h to obtain TiO_2@$(NH_2)_x$-MIL-125 core-sheath NWAs. MIL-125 is formed by the coordination of bdc with Ti-oxo clusters and constructed by connecting octahedral and tetrahedral cages.[15] $(NH_2)_x$-MIL-125 (x = 0, 1, or 2) are isostructural with each other, where NH_2-MIL-125 is synthesized by replacing bdc in MIL-125 with bdc-NH_2, while $(NH_2)_2$-MIL-125 is prepared by replacing bdc with bdc-NH_2 and bdc-$(NH_2)_2$ in a ratio of 9:1. Notably, the amino groups in the above structures are not coordinated with other inorganic components and can be accessed through triangular 5 – 7 Å windows on the cages.[16]

As depicted in Figures 1a-f and supplementary Figures S4, 5, the synthesized TiO_2@$(NH_2)_x$-MIL-125 materials possess a core-sheath structure, in which a uniform MOF sheath was constructed using an intergrown ultrathin film. By varying the concentration of the bdc-$(NH_2)_x$ ligand and titanium n-butoxide solutions, MOF sheath with varying thicknesses (~5, 15, and 100 nm) were successfully prepared on the TiO_2 NWs (Figure S5). The homogeneous MOF coating was confirmed by powder X-ray diffraction (PXRD), UV/Vis spectroscopy, X-ray photoelectron spectroscopy (XPS), fourier-transform infrared (FT-IR) spectroscopy, and transient photocurrent response measurements (Figures 1g-i and S6–13). As shown in Figures 1g and S6, 7, the diffraction peaks of TiO_2@$(NH_2)_x$-MIL-125 at 6.8°, 9.7° and 11.6° correspond with the (011), (002) and (121) faces of $(NH_2)_x$-MIL-125, respectively, whereas other peaks in the patterns (27.4, 36.1, 41.2, 54.3, 62.7 and 69.7°) are assigned to the rutile structure of TiO_2 (JCPDS No. 21–1276) and the Al_2O_3 substrate.[15,17] Figures 1h and S8 show the UV/Vis

spectra of TiO_2, $(NH_2)_x$-MIL-125 and TiO_2@$(NH_2)_x$-MIL-125 on the Al_2O_3 substrate. MIL-125 has an optical band gap in the UV region (ca. 3.3 eV/372 nm; see Figure S8a). TiO_2 and TiO_2@MIL-125 exhibit an almost identical absorption onset at 410 nm (optical band gap of ≈ 3.0 eV). A band gap decrease was observed for NH_2-MIL-125 (ca. 2.5 eV/500 nm; see Figure S8b) and $(NH_2)_2$-MIL-125 (ca. 1.3 eV/950 nm; see Figure S8c). When a bdc-NH_2 or bdc-$(NH_2)_2$ linker was used, the donation of the N 2p electrons to the aromatic linking unit resulted in a red-shifted band above the valence band edge of MIL-125.[13] Similarly, the absorption onset of TiO_2@$(NH_2)_x$-MIL-125 was red-shifted to 530 nm (ca. 2.34 eV) for $x = 1$ and 650 nm (ca. 1.90 eV) for $x = 2$, indicating that the -NH_2 functionalized linkers were key to extending the absorption band to the visible region. The absorption spectra of TiO_2@MIL-125, TiO_2@NH_2-MIL-125, and TiO_2@$(NH_2)_2$-MIL-125 are consistent with their white, yellow, and dark brown colors, respectively. The transient photocurrent response of pure TiO_2 and TiO_2@$(NH_2)_x$-MIL-125 under visible light was examined (Figure 1i). The high-power light source for the photocurrent response and gas-sensing test was a 300 W Xe lamp with a cut-off filter (420 nm < λ < 790 nm, Figure S14). TiO_2@$(NH_2)_x$-MIL-125 ($x = 1$ or 2) showed a much higher photocurrent response than pristine TiO_2 and TiO_2@MIL-125. This is consistent with the fact that the -NH_2 functional motifs on organic ligands can reduce the band gap, thus enhancing the visible light absorption of MIL-125.[16] It also reveals the synergistic effect of $(NH_2)_x$-MIL-125 ($x = 1$ or 2) and TiO_2 in promoting the separation of electron-hole pairs. Therefore, TiO_2@$(NH_2)_x$-MIL-125 exhibited a much higher photocurrent than TiO_2@MIL-125. Increasing the thickness of the MOF sheath layer could increase the photocurrent density owing to the enhanced light absorption (Figure S15), but if the MOF layer becomes too thick, the poor electron transport in the MOF layer leads to significant charge recombination, thus decreasing the photocurrent density.[18] In this work, the optimized thickness of the MOF layer resulting in the highest photoconductivity is ≈ 15 nm for TiO_2@NH_2-MIL-125.

Linear *I-V* curves of TiO_2 and TiO_2@$(NH_2)_x$-MIL-125 devices indicate good ohmic contact between the sensing materials and electrodes (Figure S16). Gas-sensing experiments were performed by placing the sensors in a sealed quartz chamber and monitoring the current change upon cyclic exposure to analytic gases and dry air at RT. In the dark, TiO_2@NH_2-MIL-125 exhibited a negligible NO_2 sensing response due to its low conductivity and few active species (Figure 2a). Under visible light, however, these sensors exhibited a reversible response to NO_2 upon cyclic exposure to NO_2 and dry air (Figure 2b). TiO_2@NH_2-MIL-125 was more sensitive than TiO_2. For example, for 100 ppm NO_2, TiO_2@NH_2-MIL-125 exhibited a response of ≈ 418 %, whereas TiO_2 had a response of only ≈ 148 % (Figure S17). As illustrated in Figures 2c, d and S17–23, we investigated the correlation between the -NH_2 groups in TiO_2@$(NH_2)_x$-MIL-125 (where $x = 0$, 1, or 2) and their sensing performance towards NO_2, focusing on sensitivity and selectivity. As shown in Figure S19, MIL-125 exhibits almost no response

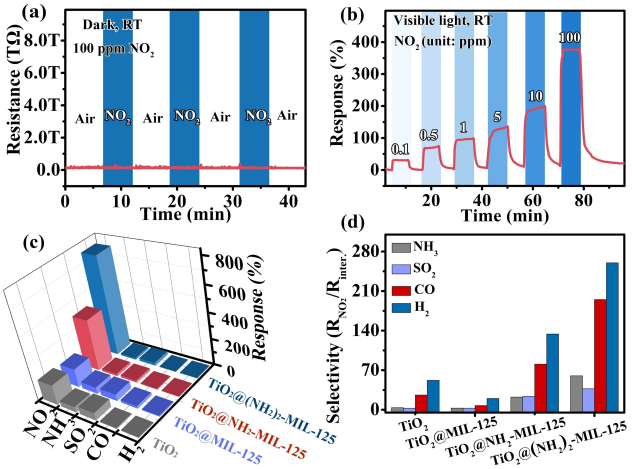

Figure 2. NO_2 gas-sensing properties of TiO_2@$(NH_2)_x$-MIL-125 sensor working at RT: (a) Dynamic response-recovery curve of TiO_2@NH_2-MIL-125 to 100 ppm NO_2 under dark; (b) Concentration-dependent dynamic response-recovery curve of TiO_2@NH_2-MIL-125 to NO_2 under visible light; (c) Comparison of the responses of TiO_2 and TiO_2@-$(NH_2)_x$-MIL-125 to the 4 analytic gases of 100 ppm at RT under visible light; (d) Enhanced selectivity of TiO_2@$(NH_2)_x$-MIL-125 compared with pris-tine TiO_2 for NO_2 gas sensor.

when used for NO_2 detection. The response value gradually increases as the amino (−NH_2) content increases. TiO_2@MIL-125 had a similar response and selectivity for NO_2 as that of pristine TiO_2. TiO_2@NH_2-MIL-125 was not only 174 % more sensitive to NO_2 detection but also 1.9–8.7 times more selective (Figure S22). The sensitivity and selectivity were further enhanced when the number of -NH_2 groups was increased using the $(NH_2)_2$-MIL-125 coating film. TiO_2@$(NH_2)_2$-MIL-125 showed the highest response of ≈ 780 % (Figure S23a). However, it suffered from slow response and incomplete recovery owing to the strong interactions between the MOF sheath and NO_2. These results indicate that the high sensitivity and good selectivity of TiO_2@$(NH_2)_x$-MIL-125 can be ascribed to the -NH_2 group in the MOF sheath. On the one hand, more -NH_2 groups result in more visible light absorption and higher photocatalytic activity, thus producing a higher response. On the other hand, compared with interfering gases, NO_2 has the strongest Lewis acid–base interaction with -NH_2; more -NH_2 groups in the MOF sheath preconcentrate more NO_2, leading to better selectivity.

Because the TiO_2@NH_2-MIL-125-based sensors have superior overall performances, they were selected for a detailed study. The thickness of the MOF sheath is one of the critical parameters controlling the sensitivity in terms of the simple diffusion reaction model.[2,19] As shown in Figure S24, for 100 ppm NO_2, the TiO_2@NH_2-MIL-125 sensor with ≈ 5, 15, and 100 nm MOF sheath has responses of 205 %, 403 %, and 117 %, respectively. Increasing the thickness of the MOF sheath could increase the adsorption of NO_2 gas. However, as the MOF layer thickens, poorer gas diffusion in MOF sheath and more unsatisfactory electron transport and charge recombination will deteriorate the sensitivity and response-recovery speeds.[18] Consistent with

the photoconductivity results, TiO_2@NH_2-MIL-125 with an ≈ 15 nm thick MOF sheath has the best sensing performance. The LOD of the sensor can be obtained from the log-log plots of response vs. concentration by setting the response to 10 %.[10] These plots show good linearity toward NO_2 concentrations in the range of 0.1–100 ppm. Accordingly, the theoretical LODs of TiO_2 and TiO_2@NH_2-MIL-125 were calculated to be 880 and 1 ppb, respectively (Figures 3a and S25). The response and recovery times of the TiO_2@NH_2-MIL-125 sensor to 100 ppm NO_2 are estimated to be 0.53 and 3.5 min, respectively (Figure S26). When the concentration of NO_2 is 0.1 ppm, the response and recovery times are as short as 0.28 and 1.3 min, respectively (Figure 3b). However, the pure NH_2-MIL-125 sensor takes 4 minutes to reach a 90 % response to 100 ppm NO_2, and only 60 % recovery can be achieved after 10 min (Figure S27). Achieving a low LOD and fast response simultaneously at RT is still a big challenge for NO_2 sensors (Table S1). To the best of our knowledge, TiO_2@NH_2-MIL-125 is the first light-activated sensor with a LOD as low as 1 ppb and a response time as short as 0.28 min (Figure 3c). The reproducibility of the TiO_2@NH_2-MIL-125 sensor was evaluated by four devices fabricated from different batches. The responses of these devices toward 100 ppm NO_2 are 400 %, 418 %, 665 %, and 468 %, respectively (Figure S28), showing good reproducibility. TiO_2@NH_2-MIL-125 was examined for six successive assays toward 1 ppm NO_2 (inset of Figure 3d). The coefficient of variation (CV) is as low as 2.9 %, indicating the good reproducibility of its response. This sensor also exhibits good long-term stability. It can work continuously for at least 1 year, with 92 % retention of its original response (Figure 3d). These results confirm that the -NH_2 group greatly affects the optical response and photocatalytic activity of MIL-125.

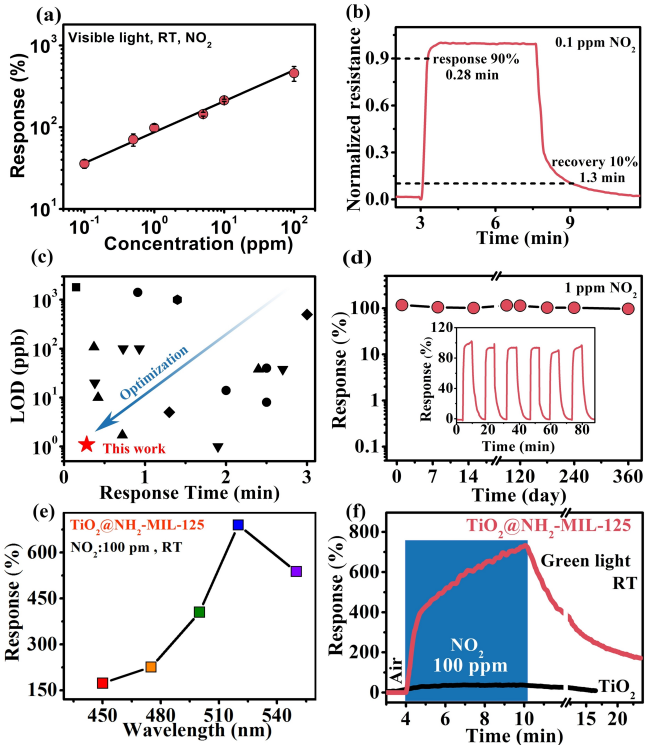

Figure 3. NO_2 gas-sensing properties of TiO_2@NH_2-MIL-125 sensor working at RT: (a) Log-log plots of response-concentration; (b) Normalized response-recovery curve to 0.1 ppm NO_2; (c) LOD and response time comparison of various light-activated NO_2 sensors at RT (●: Crystalline porous materials (MOF/COF/HOF); ▲: MOs; ▼: Metal-sulfide; : RGO-based; ◆: Perovskite; ★: This work); (d) Long-term stability (inset: the repeatability to 1 ppm NO_2). (e) Light wavelength-dependent response of TiO_2@NH_2-MIL-125 toward 100 ppm NO_2. (f) Dynamic response-recovery curves of TiO_2@NH_2-MIL-125 and pristine TiO_2 toward 100 ppm NO_2 under green light (520 nm).

Figures 3e, f and S29, 30 show the light intensity-dependent and wavelength-dependent sensing performance of the TiO_2@NH_2-MIL-125 sensor to 100 ppm NO_2 at RT. As evident in Figure S29, under visible-light irradiation, the sensor's response decreases (from 594 % to 228 %) as the light intensity increases (from 100 mW cm^{-2} to 600 mW cm^{-2}). Concurrently, the recovery capability of the sensor improves with increasing light intensity. The optimum overall performance is achieved at a visible-light intensity of approximately 400 mW cm^{-2}. Figures 3e and S30 showcase the response of the TiO_2@NH_2-MIL-125 sensor to 100 ppm NO_2 under different visible light wavelengths (450, 475, 500, 520, and 550 nm). The light intensities at these wavelengths were adjusted to be consistent. The response value initially increases from 173 % at 450 nm to 226 % at 475 nm, then rises to 405 % at 500 nm, peaks at 520 nm, and subsequently decreases to 530 % at 550 nm. At 520 nm, the maximum response of TiO_2@NH_2-MIL-125 to 100 ppm NO_2 was 2200 % higher than the response of pristine TiO_2 (Figure 3f). Although the response at the single wavelength of 520 nm is significantly higher than under visible light (420–790 nm), its response and recovery speeds are notably slower. The influence of light on gas-sensing behavior is relatively complex, and we can only make some reasonable approximations. By increasing the light intensity, the number of photogenerated charge carriers increases, enhancing the sensing activity. However, once a certain threshold is exceeded, the desorption of NO_2 from the gas-sensing material's surface significantly increases. Similarly, lower photon energies (longer wavelengths) also induce a slower desorption speed of the analyte gas, resulting in a lower recoverability.[20] In our work, for TiO_2@NH_2-MIL-125 devices used to detect NO_2 at RT, an ideal balance can be achieved among the response value, response speed, and recoverability under visible light (420–790 nm) at an intensity of 400 mW cm^{-2}.

The detailed sensing mechanism of TiO_2@$(NH_2)_x$-MIL-125 is still unclear. To verify the relationship between the amino groups of the MOF sheath and the selectivity of the TiO_2@$(NH_2)_x$-MIL-125 sensor to NO_2, we performed an ex situ XPS analysis of NH_2-MIL-125 (Figure S31). We observed a new nitrate species peak at ≈ 406.6 eV after exposure to NO_2 (*Eqs.* S7 and 8).[21] The suppression of amine-related peaks in the FT-IR spectrum (Figure S32) of NH_2-MIL-125 exposed to NO_2 also indicates its specific adsorptive interaction with NO_2.[22] This interaction is further corroborated by the gradual reduction of primary

amines (3575 and 3425 cm^{-1}) and a simultaneous increase in NO_2 (1608 cm^{-1}) and nitrite/nitrate (1388 and 1259 cm^{-1}) peaks with increasing exposure time, as evidenced by in situ FT-IR results presented in Figure S33.[23] The specific interactions of the amino groups with NO_2 are consistent with the fact that both sensitivity and selectivity improved by increasing x in pristine $(NH_2)_x$-MIL-125 or in the form of MOs@MOFs.

It has been reported that the combination of NH_2-MIL-125 and TiO_2 results in a staggered gap (type II) heterojunction, which thermodynamically allows the photogenerated charges in NH_2-MIL-125 to inject into TiO_2.[17] The heterojunction interface of the MO/MOF serves as an "electron extraction pump", improving the separation of photogenerated electrons and holes and activating TiO_2. Thus, TiO_2@$(NH_2)_x$-MIL-125 (x = 1 or 2) has a higher visible light-driven photocurrent response than TiO_2 or TiO_2@MIL-125 (Figure 1i). Electron spin resonance (ESR) spectroscopy experiments were performed to reveal more details of the electron-transport process. In the dark, negligible ESR signals were detected (Figure S34a), which agreed with the lack of response of the sensing materials to NO_2 in the dark at RT.

After visible-light irradiation, the strongest characteristic signal (g = 2.00) was observed for TiO_2@NH_2-MIL-125, indicating the existence of an abundant paramagnetic O_2^- species, which is a key active species in a sensing reaction in the MO system (Figure S34b).[24] The in situ ESR analyses further revealed that the generation of O_2^- is a Ti-mediated electron transfer process (Figure 4a). Before the measurement, the sample was evacuated to remove O_2. In this case, TiO_2@NH_2-MIL-125 changed color from yellow to dark green under light irradiation, and the characteristic values of paramagnetic Ti^{3+} centers in a distorted rhombic oxygen ligand field (g_x = 1.980, g_y = 1.953, and g_z = 1.889) were observed.[16] By contrast, without the evacuation step,

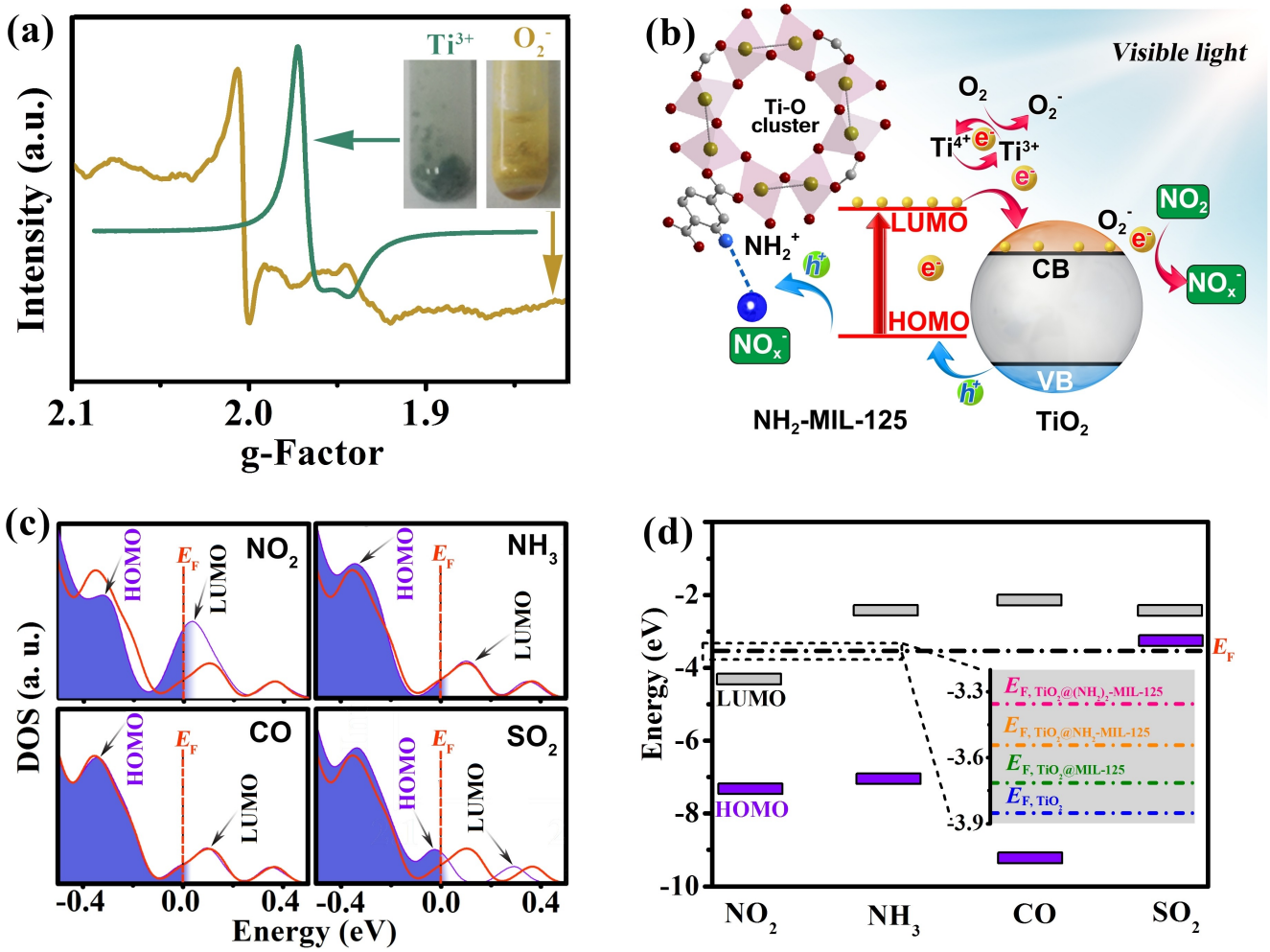

Figure 4. (a) In situ ESR spectra of TiO_2@NH_2-MIL-125 under visible light irradiation (yellow and green insets are the corresponding photographs of samples with and without oxygen, respectively). (b) Schematic illustration of the possible mechanism of the sensing reaction of TiO_2@NH_2-MIL-125 under visible light. (c) DOS of the TiO_2@NH_2-MIL-125 with adsorbed NO_2, NH_3, CO and SO_2 (The fermi levels of the different systems are set to 0 eV. For comparison, the DOS of TiO_2@NH_2-MIL-125 without any adsorbed gas molecule (red line) is shown in each graph). (d) Energy diagram of the frontier orbitals of the NO_2, NH_3, CO and SO_2 gases adsorbed on the ligand (the inset is the fermi levels of TiO_2 and TiO_2@$(NH_2)_x$-MIL-125).

TiO_2@NH_2-MIL-125 retained its yellow color, and an ESR signal associated with the O_2^- species rather than Ti^{3+} was observed. These results indicate that, in an oxygen-free atmosphere, visible light induces electron transfer to form the Ti^{3+} species. In air, however, Ti^{3+} donates electrons to O_2 to form O_2^-, followed by the reoxidation of the generated Ti^{3+} species to Ti^{4+} species. These experimental results demonstrate that when NH_2-MIL-125 is excited with visible light, an electron from its organic linker is transferred to its metal-oxo cluster via a ligand-to-metal charge transfer (LMCT) mechanism, forming Ti^{3+} (Figure 4b).[25] Subsequently, the photoexcited Ti^{3+} components of NH_2-MIL-125 inject electrons into the conduction band (CB) of TiO_2 to react with the absorbed O_2, forming the O_2^- species. The amino groups in the NH_2-MIL-125 sheath act as hole stabilizers and prolong the lifetime of the excited states in TiO_2@NH_2-MIL-125, which is beneficial for visible light photocatalytic gas sensors.[16,26] When n-type TiO_2@NH_2-MIL-125[17] is exposed to NO_2, an oxidizing and electron-withdrawing gas,[27] O_2^- is consumed and more electrons are extracted from the sensing materials.[28] These processes may effectively decrease the charge carrier concentration in TiO_2@NH_2-MIL-125 and result in sensing responses. Density functional theory (DFT) calculations reveal that, compared with other isolated gas (NH_3, SO_2 or CO)-ligand systems, only the LUMO of the NO_2-ligand system lies below the Fermi level of the TiO_2@NH_2-MIL-125 (Figures 4c, 4d and S35, 36), which indicates the energetically favorable charge transfer from TiO_2 to the LUMO of the NO_2-ligand system. This result explains the high selectivity of TiO_2@NH_2-MIL-125 to NO_2 among the interfering gases. Moreover, as shown in the inset of Figure 4d, a higher number of -NH_2 functional groups on the ligand of TiO_2@$(NH_2)_x$-MIL-125 would result in a Fermi-level shift to a higher energy level and enhance the charge transfer from TiO_2 to the LUMO of the NO_2-ligand system. Thus, TiO_2@NH_2-MIL-125 exhibits the highest response and best selectivity of the materials tested herein.

Conclusion

In summary, the precise alignment of energy levels at the interface of MOs and MOFs within MO@MOF heterojunctions has proven effective in addressing the challenge of achieving high sensitivity, unique selectivity, and rapid response at RT in one chemiresistive device. Different from the traditional core-sheath nanocomposite containing conjugated small nanoparticles, $(NH_2)_x$-MIL-125 ($x = 0$, 1, or 2) intergrown thin films were uniformly fabricated with controlled thickness on TiO_2, forming MO@MOF core-sheath NWAs. By adjusting the amino functional groups on the well-defined TiO_2@$(NH_2)_x$-MIL-125 ($x = 0$, 1, or 2) interface, we transformed the heterojunction interface from a straddling gap to a staggered gap type. Due to such an energy level aligned interface, the core-sheath heterostructures can combine the advantages of both and bring additional synergistic effects to improve the gas sensing properties. This enabled the generation of active oxygen species under visible light, significantly lowering the operating temperature to RT. Detailed studies on the sensing performances of TiO_2@$(NH_2)_x$-MIL-125 ($x = 0$, 1, or 2) revealed that increasing -NH_2 groups significantly improved the response and selectivity to NO_2. Specifically, TiO_2@NH_2-MIL-125 demonstrated excellent comprehensive gas-sensing performances for NO_2 detection, including a LOD at the ppb-level, response time in the second-level, long-term stability over years and good selectivity. These findings could pave the way for designing sensing materials with excellent comprehensive performance through MOF-MO cooperation.

Acknowledgements

This work was financially supported by the National Natural Science Foundation of China (91961115, 22171263,, 22475046, 22494633, and 22325109), Self-deployment Project Research Program of Haixi Institutes, Chinese Academy of Sciences (CXZX-2022-GH09), Scientific Research and Equipment Development Project of CAS (YJ-KYQ20210024), the research fund of State Key Laboratory of Mesoscience and Engineering (MESO-23-A07, MESO-23-T02), Fujian Science & Technology Innovation Laboratory for Optoelectronic Information of China (2021ZR101), Natural Science Foundation of Fujian Province (2024 J01455), and the Fujian Education Department Project (JAT231011). We would like to express our sincere gratitude to Prof. Hexiang Deng and Dr. Chao Wang from Wuhan University for providing the SEM images of TiO_2@NH_2-MIL-125 and for conducting the C, N, O, and Ti EDX mapping measurements.

Conflict of Interest

The authors declare no competing financial interests.

Data Availability Statement

The data that support the findings of this study are available from the corresponding author upon reasonable request.

Keywords: energy level alignment · MO@MOF interface · electrical device · high-performance NO_2 detection

[1] a) A. Sharma, S. B. Eadi, H. Noothalapati, M. Otyepka, H.-D. Lee, K. Jayaramulu, *Chem. Soc. Rev.* **2024**, *53*, 2530–2577; b) S. Park, M. Kim, Y. Lim, D. Oh, J. Ahn, C. Park, S. Woo, W. Jung, J. Kim, I.-D. Kim, *Adv. Mater.* **2024**, 2313731.

[2] J. Zhang, X. Liu, G. Neri, N. Pinna, *Adv. Mater.* **2016**, *28*, 795–831.

[3] a) J. Kong, N. R. Franklin, C. W. Zhou, M. G. Chapline, S. Peng, K. J. Cho, H. J. Dai, *Science* **2000**, *287*, 622–625; b) B. Yang, N. V. Myung, T. T. Tran, *Adv. Electron. Mater.* **2021**, *7*, 2100271.

[4] a) T. Song, X. Cai, M. W.-Y. Tu, X. Zhang, B. Huang, N. P. Wilson, K. L. Seyler, L. Zhu, T. Taniguchi, K. Watanabe, M. A. McGuire, D. H. Cobden, D. Xiao, W. Yao, X. Xu, *Science* **2018**, *360*, 1214–1218; b) Y. Yoon, Z. Lu, C. Uzundal, R. Qi, W. Zhao, S. Chen, Q. Feng, W. Kim, M. H. Naik, K. Watanabe, T. Taniguchi, S. G. Louie, M. F. Crommie, F. Wang, *Nature* **2024**, *631*, 771–776; c) D. Bekermann, A. Gasparotto, D. Barreca, C. Maccato, E. Comini, C. Sada, G. Sberveglieri, A. Devi, R. A. Fischer, *ACS Appl. Mater. Interfaces* **2012**, *4*, 928–934.

[5] a) J. F. Sierra, J. Fabian, R. K. Kawakami, S. Roche, S. O. Valenzuela, *Nat. Nanotechnol.* **2021**, *16*, 856–868; b) W. He, D. Wu, L. Kong, P. Yu, G. Yang, *Adv. Mater.* **2024**, *36*, 2312541; c) L. Zhang, J. Zhang, H. Yu, J. Yu, *Adv. Mater.* **2022**, *34*, 2107668; d) G. Pasquale, Z. Sun, G. Migliato Marega, K. Watanabe, T. Taniguchi, A. Kis, *Nat. Nanotechnol.* **2024**, *19*, 941–947.

[6] a) L. Wang, S. Papadopoulos, F. Iyikanat, J. Zhang, J. Huang, T. Taniguchi, K. Watanabe, M. Calame, M. L. Perrin, F. J. G. de Abajo, L. Novotny, *Nat. Mater.* **2023**, *22*, 1094–1099; b) R. Lin, Y. Wang, Q. Lu, B. Tang, J. Li, H. Gao, Y. Gao, H. Li, C. Ding, J. Wen, P. Wu, C. Liu, S. Zhao, K. Xiao, Z. Liu, C. Ma, Y. Deng, L. Li, F. Fan, H. Tan, *Nature* **2023**, *620*, 994–1000; c) J. Miao, C. Leblanc, J. Wang, Y. Gu, X. Liu, B. Song, H. Zhang, S. Krylyuk, W. Hu, A. V. Davydov, T. Back, N. Glavin, D. Jariwala, *Nat. Electron.* **2022**, *5*, 744–751.

[7] a) S. Mondal, R. Sahoo, J. Behera, M. C. Das, *Coord. Chem. Rev.* **2024**, *514*, 215924; b) G. Cai, P. Yan, L. Zhang, H.-C. Zhou, H.-L. Jiang, *Chem. Rev.* **2021**, *121*, 12278–12326; c) D.-W. Lim, H. Kitagawa, *Chem. Soc. Rev.* **2021**, *50*, 6349–6368; d) B. Pramanik, R. Sahoo, M. C. Das, *Coord. Chem. Rev.* **2023**, *493*, 215301; e) K. Shen, L. Zhang, X. Chen, L. Liu, D. Zhang, Y. Han, J. Chen, J. Long, R. Luque, Y. Li, B. Chen, *Science* **2018**, *359*, 206–210; f) Z. Zheng, H. L. Nguyen, N. Hanikel, K. K.-Y. Li, Z. Zhou, T. Ma, O. M. Yaghi, *Nat. Protoc.* **2023**, *18*, 136–156.

[8] a) H.-Y. Li, S.-N. Zhao, S.-Q. Zang, J. Li, *Chem. Soc. Rev.* **2020**, *49*, 6364–6401; b) S. Lee, E. A. Kapustin, O. M. Yaghi, *Science* **2016**, *353*, 808–811; c) *Nat. Chem.* **2016**, *8*, 987–987; d) X. Cui, K. Chen, H. Xing, Q. Yang, R. Krishna, Z. Bao, H. Wu, W. Zhou, X. Dong, Y. Han, B. Li, Q. Ren, M. J. Zaworotko, B. Chen, *Science* **2016**, *353*, 141–144.

[9] a) Z. Wang, X. Yue, Q. Xiang, *Coord. Chem. Rev.* **2024**, *504*, 215674; b) Z. Wang, X.-M. Shi, F.-Z. Chen, G.-C. Fan, W.-W. Zhao, *Adv. Funct. Mater.* **2024**, 2404497.

[10] M.-S. Yao, W.-X. Tang, G.-E. Wang, B. Nath, G. Xu, *Adv. Mater.* **2016**, *28*, 5229–5234.

[11] W.-H. Deng, M.-S. Yao, M.-Y. Zhang, M. Tsujimoto, K. Otake, B. Wang, C.-S. Li, G. Xu, S. Kitagawa, *Natl. Sci. Rev.* **2022**, *9*, nwac143.

[12] a) A. Modi, N. Koratkar, E. Lass, B. Q. Wei, P. M. Ajayan, *Nature* **2003**, *424*, 171–174; b) L. J. Small, S. E. Henkelis, D. X. Rademacher, M. E. Schindelholz, J. L. Krumhansl, D. J. Vogel, T. M. Nenoff, *Adv. Funct. Mater.* **2020**, *30*, 2006598; c) J.-H. Kim, A. Mirzaei, H. W. Kim, S. S. Kim, *ACS Appl. Mater. Interfaces* **2019**, *11*, 24172–24183; d) D. Barreca, D. Bekermann, E. Comini, A. Devi, R. A. Fischer, A. Gasparotto, C. Maccato, C. Sada, G. Sberveglieri, E. Tondello, *CrystEngComm* **2010**, *12*, 3419–3421; e) D. Peeters, D. Barreca, G. Carraro, E. Comini, A. Gasparotto, C. Maccato, C. Sada, G. Sberveglieri, *J. Phys. Chem. C* **2014**, *118*, 11813–11819.

[13] C. H. Hendon, D. Tiana, M. Fontecave, C. Sanchez, L. D'Arras, C. Sassoye, L. Rozes, C. Mellot-Draznieks, A. Walsh, *J. Am. Chem. Soc.* **2013**, *135*, 10942–10945.

[14] B. Liu, E. S. Aydil, *J. Am. Chem. Soc.* **2009**, *131*, 3985–3990.

[15] M. Dan-Hardi, C. Serre, T. Frot, L. Rozes, G. Maurin, C. Sanchez, G. Ferey, *J. Am. Chem. Soc.* **2009**, *131*, 10857–10859.

[16] M. B. Chambers, X. Wang, L. Ellezam, O. Ersen, M. Fontecave, C. Sanchez, L. Rozes, C. Mellot-Draznieks, *J. Am. Chem. Soc.* **2017**, *139*, 8222–8228.

[17] J. W. Yoon, D. H. Kim, J.-H. Kim, H. W. Jang, J.-H. Lee, *Appl. Catal. B* **2019**, *244*, 511–518.

[18] L. Zhang, P. Cui, H. Yang, J. Chen, F. Xiao, Y. Guo, Y. Liu, W. Zhang, F. Huo, B. Liu, *Adv. Sci.* **2016**, *3*, 1500243.

[19] T. Becker, S. Ahlers, C. Bosch-vonBraunmühl, G. Müller, O. Kiesewetter, *Sens. Actuators B* **2001**, *77*, 55–61.

[20] a) A. Gaiardo, B. Fabbri, A. Giberti, V. Guidi, P. Bellutti, C. Malagu, M. Valt, G. Pepponi, S. Gherardi, G. Zonta, A. Martucci, M. Sturaro, N. Landini, *Sens. Actuators B* **2016**, *237*, 1085–1094; b) Q. Geng, Z. He, X. Chen, W. Dai, X. Wang, *Sens. Actuators B* **2013**, *188*, 293–297; c) L. Guo, Z. Yang, X. Dou, *Adv. Mater.* **2017**, *29*, 1604528.

[21] a) S.-J. Choi, J.-S. Jang, H. J. Park, I.-D. Kim, *Adv. Funct. Mater.* **2017**, *27*, 1606026; b) G. W. Peterson, J. J. Mahle, J. B. DeCoste, W. O. Gordon, J. A. Rossin, *Angew. Chem. Int. Ed.* **2016**, *55*, 6235–6238; c) J. A. Rodriguez, T. Jirsak, G. Liu, J. Hrbek, J. Dvorak, A. Maiti, *J. Am. Chem. Soc.* **2001**, *123*, 9597–9605.

[22] S. Friebe, A. Mundstock, D. Unruh, F. Renz, J. Caro, *J. Membr. Sci.* **2016**, *516*, 185–193.

[23] E. Ozensoy, D. Herling, J. Szanyi, *Catal. Today* **2008**, *136*, 46–54.

[24] E. Comini, *Mater. Today* **2020**, *7*, 100099.

[25] a) Y. Fu, L. Sun, H. Yang, L. Xu, F. Zhang, W. Zhu, *Appl. Catal. B* **2016**, *187*, 212–217; b) M. Martis, K. Mori, K. Fujiwara, W.-S. Ahn, H. Yamashita, *J. Phys. Chem. C* **2013**, *117*, 22805–22810.

[26] J. G. Santaclara, M. A. Nasalevich, S. Castellanos, W. H. Evers, F. C. M. Spoor, K. Rock, L. D. A. Siebbeles, F. Kapteijn, F. Grozema, A. Houtepen, J. Gascon, J. Hunger, M. A. van der Veen, *ChemSusChem* **2016**, *9*, 388–395.

[27] a) D. Barreca, A. Gasparotto, C. Maccato, C. Maragno, E. Tondello, E. Comini, G. Sberveglieri, *Nanotechnology* **2007**, *18*, 125502; b) M. Donarelli, S. Prezioso, F. Perrozzi, F. Bisti, M. Nardone, L. Giancaterini, C. Cantalini, L. Ottaviano, *Sens. Actuators B* **2015**, *207*, 602–613.

[28] a) X. Wang, N. Aroonyadet, Y. Zhang, M. Meckenburg, X. Fang, H. Chen, E. Goo, C. Zhou, *Nano Lett.* **2014**, *14*, 3014–3022; b) D. Barreca, E. Comini, A. Gasparotto, C. Maccato, C. Maragno, G. Sberveglieri, E. Tondello, *J. Nanosci. Nanotechnol.* **2008**, *8*, 1012–1016.

Manuscript received: October 5, 2024
Accepted manuscript online: December 5, 2024
Version of record online: December 13, 2024